Truly Distributed and Ultra-Fast Microwave Photonic Fiber-Optic Sensor

Dengwang Zhou, *Student Member, OSA*, Yongkang Dong, *Member, IEEE, Member, OSA*, and Jianping Yao, *Fellow, IEEE, Fellow, OSA*

***Abstract*—Brillouin-based optical fiber sensing has gained considerable attention for the past few years thanks to its ability to offer distributed sensing. The major limitation of a Brillouin-based optical fiber sensor is its complexity because a time-consuming frequency-sweeping process is needed to obtain a local Brillouin gain spectrum (BGS) and to calculate the local Brillouin frequency shift (BFS). Thus, it is only suitable for static or slow-varying measurements. In this article, we propose an approach to achieve truly distributed and ultra-fast fiber-optic sensing based on an active and distributed bandpass microwave photonic filter (MPF) through stimulated Brillouin scattering (SBS). To obtain a truly distributed BFS, a counter-propagating single-shot pump pulse is launched into the fiber link and a microwave multi-tone (MMT) signal with a random initial phase distribution which is phase modulated on an optical carrier is launched into the fiber link from the other end. Due to the SBS effect, the -1st order sideband of the phase-modulated signal will experience Brillouin amplification while the $+1$st order sideband will experience Brillouin attenuation, and the phase-modulated signal is converted to an intensity-modulated signal. The entire operation is equivalent to a bandpass MPF. By detecting the optical signal at a photodetector (PD), a regenerated MMT signal with its magnitude and phase that are shaped by the MPF is obtained. By evaluating the regenerated MMT signal, the Brillouin information corresponding to the temperature or strain change at a specific location is revealed. The major advantage of the approach is that time-consuming frequency-sweeping process is avoided. Truly distributed strain, temperature, and vibration sensing with a 2 m spatial resolution over 49.5 m distance at a speed up to 83.3 kHz is experimentally demonstrated.**

***Index Terms*—Microwave photonics, microwave filters, optical fiber sensors, temperature sensors.**

Manuscript received September 18, 2019; revised December 19, 2019 and February 29, 2020; accepted March 16, 2020. Date of publication March 19, 2020; date of current version July 23, 2020. This work was supported by the Natural Sciences and Engineering Research Council of Canada. The work of D. Zhou was supported by the China Scholarship Council under a scholarship. *(Corresponding author: Jianping Yao.)*

Dengwang Zhou is with the Microwave Photonics Research Laboratory, School of Electrical Engineering and Computer Science, University of Ottawa, Ottawa, ON K1N6N5, Canada, and also with the National Key Laboratory of Science and Technology on Tunable Laser, Harbin Institute of Technology, Harbin 150001, China (e-mail: dzhou059@uottawa.ca).

Yongkang Dong is with the National Key Laboratory of Science and Technology on Tunable Laser, Harbin Institute of Technology, Harbin 150001, China (e-mail: aldendong@gmail.com).

Jianping Yao is with the Microwave Photonics Research Laboratory School of Electrical Engineering and Computer Science, University of Ottawa, Ottawa, ON K1N 6N5, Canada (e-mail: jpyao@uottawa.ca).

Color versions of one or more of the figures in this article are available online at http://ieeexplore.ieee.org.

Digital Object Identifier 10.1109/JLT.2020.2982063

I. Introduction

FIBER-OPTIC sensors have widely been researched in the last few decades which can find numerous applications such as health monitoring of civil infrastructure, geological hazards prevention and perimeter security protection [1]–[4]. In a distributed fiber-optic sensor, an optical fiber usually plays two roles: as a light transmission medium and as a distributed sensing element. Stimulated Brillouin scattering (SBS) [5], a prominent nonlinear-optical effect, is usually considered as a superior mechanism employed for optical fiber sensing because it can provide high accuracy and long-distance sensing [6], [7]. Generally, Brillouin-based optical fiber sensing is realized by using two counter-propagating optical waves, one as a pump and the other as a probe. When the frequency offset of the two optical waves is close to the Brillouin frequency shift (BFS) $\nu_B \sim 11$ GHz [8], the energy of the high-frequency pump will be transferred to the low-frequency probe leading to effective narrowband amplification. Since the BFS corresponding to the central frequency of the Brillouin gain (or loss) spectrum (BGS or BLS) is temperature or strain sensitive, by monitoring the BFS change, the temperature or strain can be measured. The major limitation of the approach is that a time-consuming frequency-sweeping process is required to obtain the BGS or BLS. To quickly measure the distributed BGS or BLS, several Brillouin-based approaches have been proposed in which the measurements are done based on the SBS interaction in the optical correlation domain [9]–[12] and the optical time domain [13]–[20].

For the optical correlation-domain approach, two frequency or phase periodically modulated optical waves are counter-propagating from the two ends of a sensing fiber, which is referred to as an analysis scheme. A series of discrete correlation peaks are generated at the locations where the SBS occurs, and the locations of these peaks can be swept by controlling the time delay difference or the modulation frequency between two frequency-modulated optical waves for truly distributed sensing [9]. By sweeping the center frequency difference between the two frequency-modulated optical waves, the corresponding BGS can be obtained. An analysis scheme was implemented to detect a 200-Hz point vibration with a spatial resolution of 10 cm and a sampling rate of 1 kHz [10]. Dynamic strain measurements at arbitrary five points were obtained simultaneously at a sampling rate of 5,000 Hz with random accessibility by using a voltage-controlled oscillator to sweep the BGS and a higher-speed lock-in amplifier to acquire the data [11]. Then, a truly distributed vibration measurement along a 100-m optical fiber was realized with a sampling rate of 20 Hz via differential frequency-modulating pump wave and probe wave to repeatedly sweep the peak location [12]. However, for these schemes, the truly distributed dynamic measurements were realized by both the frequency-sweeping and the position scanning process, which is again time-consuming and severely limits the sensing speed.

For the optical time-domain approach, Brillouin optical time-domain analysis (BOTDA) is widely reported. Typically, a distributed Brillouin signal can be obtained with a pulsed-pump and a counter-propagated continuous single-tone probe wave, and the position information can be easily identified through the round-trip time of the pump pulse which can avoid the position scanning process. Then, the distributed BGS can be achieved by sweeping the frequency difference between the pump pulse and the probe wave. To increase the sampling rate, techniques such as optical frequency-agile (OFA) technique [13], slope-assisted (SA) method [14], [15], orthogonal frequency-division multiplexing (OFDM) modulation [16], [17], [21] as well as digital optical frequency comb (DOFC) modulation [18], [19], and optical chirp chain (OCC) modulation [20] have been proposed and demonstrated. In the OFA technique, a combination of a 500 MHz arbitrary waveform generator (AWG) and a microwave vector signal generator was employed to generate an electrical frequency-agile signal resulting in fast switching of the optical frequency [13]. A distributed measurement of vibration with a frequency of 100 Hz along a 100-m fiber was achieved at a 10-kHz sampling rate, which was reported in reference [13]. However, the maximum sampling rate of this technique is still limited by the frequency-sweeping process. In the SA technique [14], the distributed BFS can be directly demodulated via the intensity of the Brillouin signal by setting the frequency of the probe wave at the middle of the slope of the BGS, which does not need the frequency-sweeping process. Without averaging, the maximum sampling rate of this technique is basically limited by the round-trip time of pump pulse with respect to the length of the sensing fiber, but the dynamic range is close to the linewidth of the BGS about 35 MHz ($\sim$700 $\mu\varepsilon$) [14]. To extend the dynamic range, an improved SA-BOTDA was implemented via the OFA technique to generate the frequency-agile probe segments corresponding to multiple slopes, which can increase the dynamic range up to 241 MHz ($\sim$5000 $\mu\varepsilon$) but sacrifice the sampling rate as it is inversely proportional to the number of the slopes in this approach [15]. In the OFDM method, an OFDM signal was used to generate a dual-polarization probe wave so that the polarization fading in a single-mode fiber can be eliminated leading to a long-distance measurement without the need for averaging. Then, a BGS can be obtained by just launching a single-shot pump pulse into the sensing fiber to interact with a complete broadband OFDM symbol, and the symbol period is inversely proportional to the subcarrier frequency spacing so as to recover the OFDM information symbol without intercarrier interference (ICI) [16], [21]. Furthermore, the BGS distribution can be obtained for a broadband OFDM probe wave that contains a large number of OFDM symbols in series. Although the maximum sampling rate of this technique is only limited by the fiber length, the spatial resolution is limited by the symbol period of the OFDM symbol, corresponding to tens of meters [16], [17] which is too wide to meet the requirement for practical applications. In the OCC method, an electrical broadband frequency-agile signal whose duration is compressed to 20 ns was used to modulate the probe wave into a short optical chirp segment in which a BGS can be revealed by also counter-propagating a single-shot pump pulse. Then, the BGS distribution can be realized for an optical chirp chain probe wave that cascaded by several short optical chirp segments by a head-to-tail cohesion. A sampling rate up to MHz and a spatial resolution of 2 m had been experimentally demonstrated [20]. However, the BGS distribution in both the OFDM-based technique and the OCC-based technique are arranged symbol-by-symbol (or segment by segment), only quasi-distribution measurement is possible and the Brillouin information between two symbols cannot be demodulated. To sum up, the state-of-the-art approaches mentioned above have some trade-offs for truly distributed sensing, including measurement speed, dynamic range, and spatial resolution.

In this paper, we propose a novel microwave photonic fiber-optic sensor based on a distributed bandpass microwave photonic filter (MPF [22]–[24]) to achieve truly distributed and ultra-fast measurements with a wide dynamic range and a high spatial resolution. A continuous-wave probe wave in the sensing fiber is phase-modulated by a microwave multi-tone (MMT) signal to generate an optical carrier and $\pm$1st order sidebands. For a phase modulated signal if detected directly by a photodetector (PD), since the beating between the optical carrier and the $+$1st order sideband and the beating between the optical carrier and the $-$1st order sideband have a π phase difference, the two beat signals will fully cancel, and no microwave signal is detected. Due to the SBS effect, however, the $-$1st order sideband of the phase-modulated signal will experience Brillouin amplification while the $+$1st order sideband will experience Brillouin attenuation, the phase-modulated signal is converted to an intensity-modulated signal [25]. The entire operation is equivalent to a bandpass MPF. By detecting the optical signal at a PD, a regenerated MMT signal with its magnitude and phase that are shaped by the MPF is obtained. By evaluating the MMT signal, the Brillouin information corresponding to the temperature or strain change along the sensing fiber is revealed. Without averaging, the sampling rate of the proposed sensor is only limited by the round-trip time of the pump pulse with respect to the length of the sensing fiber, and the dynamic range can be easily tuned by changing the bandwidth of the MMT signal. To test the performance of the proposed sensor, an experiment for static temperature, strain, and vibration measurement is performed. The results show that high spatial resolution sensing of 2 m over 49.5 m distance at a maximum sampling rate of 83.3 kHz is achieved.

II. Principle

A. Operation Principle

The proposed sensor is implemented based on an active and distributed bandpass MPF. As shown in Fig. 1(a), both a pulsed-pump and a continuous probe wave are counter-propagated

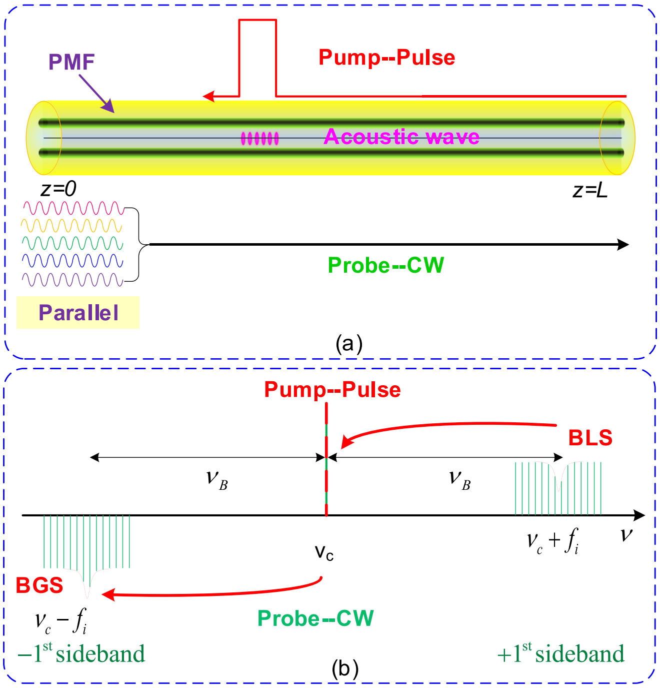

Fig. 1. Operation principle of the proposed sensor. (a) The time relationship between the pump pulse and the continuous probe wave; (b) The frequency relationship between the pump pulse and the phase-modulated probe wave. BGS: Brillouin gain spectrum; BLS: Brillouin loss spectrum; PMF: polarization maintaining fiber.

into a Panda type polarization-maintaining fiber (PMF) used as the sensing fiber to avoid the polarization-dependent fading. The two waves can interact with each other through an acoustic wave due to the SBS effect when their frequency difference is close to the BFS of the PMF. Unlike a conventional BOTDA system with a single-tone probe wave and the OFDM technique using discrete symbols, a continuous and broadband MMT signal with multiple tones is used. The MMT signal is modulated on the probe wave by phase modulation with a small modulation index, to generate an optical carrier and $\pm$1st order sidebands. By detecting the phase-modulated probe wave without the pump pulse, no microwave is recovered due to the cancellation of the two-beat signals. As shown in Fig. 1(b), with a pump pulse that has a frequency equal to that of the optical carrier, the upper sideband of the phase-modulated probe wave is attenuated and the lower sideband is amplified, so that phase-modulation to intensity-modulation conversion for the probe wave is realized. As a result, a regenerated MMT signal containing the local environmental information is obtained by detecting the probe wave. The entire operation is equivalent to an active and distributed bandpass MPF whose local passband is dependent on the local BGS and the power spectrum of the transmitting pump pulse. By making a time-frequency analysis of the regenerated MMT signal, the distribution of the BGS and its BFS can be demodulated. The maximum sampling rate of the proposed sensor is only limited by the repetition rate of the single-shot pump pulse corresponding to the length of the PMF.

An MMT signal with a random initial phase distribution is generated by an AWG. Random initial phase distribution is needed to lower the peak to average power ratio (PAPR) and a more random time-frequency relation. Mathematically, the MMT signal is given

$$y_{\mathrm{MMT}}(t) = \sum_{i=1}^{N} V_0 \sin(2\pi f_i t + \varphi_i) \tag{1a}$$

$$\varphi_i = \mathrm{random}\{0, 2\pi\} \tag{1b}$$

where $f_i = f_0 + (i-1)\Delta f$ is the frequency of the i^{th} tone and Δf is the frequency interval between two adjacent tones, φ_i is the initial phase of the i^{th} tone, V_0 and N are amplitude and tone number of the MMT signal, respectively. Then, the MMT signal is applied to a phase modulator (PM) to phase-modulate the continuous probe wave. The phase-modulated probe wave is given by

$$\begin{aligned} E_{\mathrm{PM}}(t) &= E_0 \exp\left[j2\pi\nu_0 t + \sum_{i=1}^{N} j\gamma \sin(2\pi f_i t + \varphi_i)\right] \\ &= E_0 \exp(j2\pi\nu_c t)\prod_{i=1}^{N}\exp\left[j\gamma\sin(2\pi f_i t + \varphi_i)\right] \\ &= E_0 \exp(j2\pi\nu_c t)\prod_{i=1}^{N}\sum_{m=-\infty}^{\infty} J_m(\gamma) \\ &\quad \times \exp\left[jm(2\pi f_i t + \varphi_i)\right] \end{aligned} \tag{2}$$

where E_0 and ν_c are the amplitude of the electric field and the frequency of the optical carrier, respectively; $j = \sqrt{-1}$; $J_m(\gamma)$ is the m^{th} order Bessel function of the first kind, $\gamma = \pi V_0/V_\pi$ is the modulation index, and $V_\pi$is the half-wave voltage of the PM.

For a small modulation index, the 2nd order sideband and the higher-order sidebands are small and can be ignored. As the modulation index increases, the 2nd order and the higher-order sidebands will be excited, resulting in a severe RF noise, which can be eliminated by a digital passband filter. Therefore, we just consider an optical carrier and $\pm$1st order sidebands (i.e., $m = 0, \pm 1$). Then, Eq. (2) is simplified as

$$\begin{aligned} E_{\mathrm{PM}}(t) &= E_0 J_0^N(\gamma)\exp(j2\pi\nu_c t) \\ &\quad - E_0 J_1(\gamma)\sum_{i=1}^{N}\exp\left[j2\pi(\nu_c - f_i t) - j\varphi_i\right] \\ &\quad + E_0 J_1(\gamma)\sum_{i=1}^{N}\exp\left[j2\pi(\nu_c + f_i t) + j\varphi_i\right] \end{aligned} \tag{3}$$

Since the beat signals generated by the optical carrier and the $\pm$1st sidebands are equal in magnitude but out of phase, no microwave signal is detected at a PD. When both the pump pulse and the phase-modulated probe wave are launched into the PMF, the phase cancellation condition is no longer maintained due to the Brillouin amplification for the $-$1st order sideband and the Brillouin attenuation for the +1st order sideband. Then, the output is given by

$$\begin{aligned} E'_{\mathrm{PM}}(t) &= E_0 J_0^N(\gamma)\exp(j2\pi\nu_c t) \\ &- E_0 J_1(\gamma)\sum_{i=1}^{N} H_{\mathrm{BGS}}(f_i,z)\exp[j2\pi(\nu_c - f_i t) - j\varphi_i] \\ &+ E_0 J_1(\gamma)\sum_{i=1}^{N} H_{\mathrm{BLS}}(f_i,z)\exp[j2\pi(\nu_c + f_i t) + j\varphi_i] \end{aligned} \tag{4}$$

where the $H_{\mathrm{BGS}}(f_i, z)$ and $H_{\mathrm{BLS}}(f_i, z)$ are the complex BGS and the complex BLS at position z, respectively, which are given

$$H_{\mathrm{BGS-BLS}}(f_i, z) = \exp\left\{\frac{\pm g_0 \Delta\nu_B}{\Delta\nu_B + 2j[f_i - \nu_B(z)]}\right\} \tag{5}$$

where $+$ and $-$ correspond to the complex BGS and BLS, respectively; g_0 is the peak gain, $\nu_B(z)$ is the local BFS of the PMF, and $\Delta\nu_B$ is the linewidth of the BGS. Then, (5) can be approximated by [26]

$$H_{\mathrm{BGS-BLS}}(f_i, z) \approx (1 \pm G_{\mathrm{SBS}}(f_i, z))\exp(\pm j\varphi_{\mathrm{SBS}}(f_i, z)) \tag{6}$$

where $G_{\mathrm{SBS}}(f_i, z)$ and $\varphi_{\mathrm{SBS}}(f_i, z)$ are the BGS and the Brillouin phase-shift spectrum (BPS), respectively, which are given by

$$G_{\mathrm{SBS}}(f_i, z) = \frac{g_0 \Delta\nu_B^2}{\Delta\nu_B^2 + 4[f_i - \nu_B(z)]^2} \tag{7a}$$

$$\varphi_{\mathrm{SBS}}(f_i, z) = -\frac{2g_0 \Delta\nu_B [f_i - \nu_B(z)]}{\Delta\nu_B^2 + 4[f_i - \nu_B(z)]^2} \tag{7b}$$

When the phase-modulated optical probe wave is received at a high-speed PD, an MMT signal is regenerated, which is given by

$$y_{\mathrm{R}}(t) \propto R_{\mathrm{D}} \sum_{i=1}^{N} G_{\mathrm{SBS}}(f_i, z)\ \cos(2\pi f_i t + \varphi_i - \varphi_{\mathrm{SBS}}) \tag{8}$$

where R_{D} is the responsivity of the PD.

B. Transfer Function of the Active Bandpass MPF

As the pump pulse is propagating over the sensing fiber, the transfer function of the MPF at position z can be expressed as

$$|H(f_i, z)| \propto G_{\mathrm{SBS}}(f_i, z) * P_{\mathrm{Pump\_pulse}}(f_i) \tag{9}$$

where $P_{\mathrm{Pump_pulse}}(f_i, z)$is the power spectrum of the pump pulse, and $*$ is the convolution operator.

C. Demodulation Process

Different from the OFDM technique which needs a complex demodulation process such as synchronization, fast Fourier transform (FFT), and channel estimation [16], the time-frequency analysis of the regenerated MMT in our proposed sensor will be calculated simply by a short-time Fourier transform (STFT). Finally, a reconstructed BGS is obtained, given by

$$G'_{\mathrm{SBS}}(f_i, z) = G_{\mathrm{SBS}}(f_i, z) * P_{\mathrm{Pump\_pulse}}(f_i) * P_{\mathrm{window}}(f_i) \tag{10}$$

where $P_{window}(f_i)$is the spectrum of a time window for the STFT.

The center frequency of the reconstructed BGS corresponding to the BFS of the local PMF is a function of the strain and temperature [1],

$$\nu_B(z) = \nu_{B0}(z) + C_\varepsilon \Delta\varepsilon(z) + C_{\mathrm{T}}\Delta T(z) \tag{11}$$

where $\nu_{B0}(z)$, $\Delta\varepsilon(z)$and $\Delta T(z)$are the initial BFS, the strain change and the temperature change at position z, respectively. C_ε and C_T are the strain and temperature coefficients of the sensing fiber, respectively.

The measurement speed of the proposed sensor is given by

$$f_{\mathrm{frame}} = \frac{1}{T_{\mathrm{round\_trip}} N_{\mathrm{averge}}} \tag{12}$$

where $T_{\mathrm{round\_trip}}$ is the round-trip flight time over the sensing fiber for the pump pulse, which is given by $T_{\mathrm{round\_trip}} = 2n_{eff}L/c$, n_{eff} is the effective refractive index of the sensing fiber core, L is the length of the sensing fiber, and c is the speed of light in vacuum. N_{averge} is the number of times of averaging. Without averaging, the distributed BGS along the sensing fiber can be obtained by injecting a single-shot pump pulse so that the maximum measurement speed of the proposed distributed sensor is only limited by the fiber length, making the sensor ultra-fast.

D. Spatial Resolution

Different from an OFDM probe wave or an OCC probe wave which is formed by cascading some symbols, thus it is only able to demodulate one BGS per symbol. For the proposed approach, however, the input MMT signal consisting of multiple sinusoidal waves with a randomized initial phase distribution is continuous in time, thus the time window for calculating the STFT can be moved forward continuously, i.e., truly distributed measurement is possible. The spatial resolution of the proposed microwave photonic fiber-optic sensor is given by

$$\Delta z = \frac{c\Delta t_{\mathrm{p}}}{2n_{\mathrm{eff}}} + \frac{c\Delta t_{\mathrm{window}}}{2n_{\mathrm{eff}}} \tag{13}$$

where Δt_{p} is the width of the pump pulse, $\Delta t_{\mathrm{window}}$ is the time window of the STFT. The first term in the right-hand side is the spatial coverage of the pump pulse, and the second term in the right-hand side is the spatial coverage of the time window of the STFT. The interval of the demodulated spatial point is determined by the parameters of the STFT algorithm.

III. Experimental Setup

Fig. 2 depicts the schematic diagram of the microwave photonic fiber-optic sensor. A continuous-wave (CW) laser diode (LD) operating at 1550.054 nm with an output power of 15 dBm is employed as a light source. The output light is split into two branches by a 50:50 optical coupler (OC), with the light

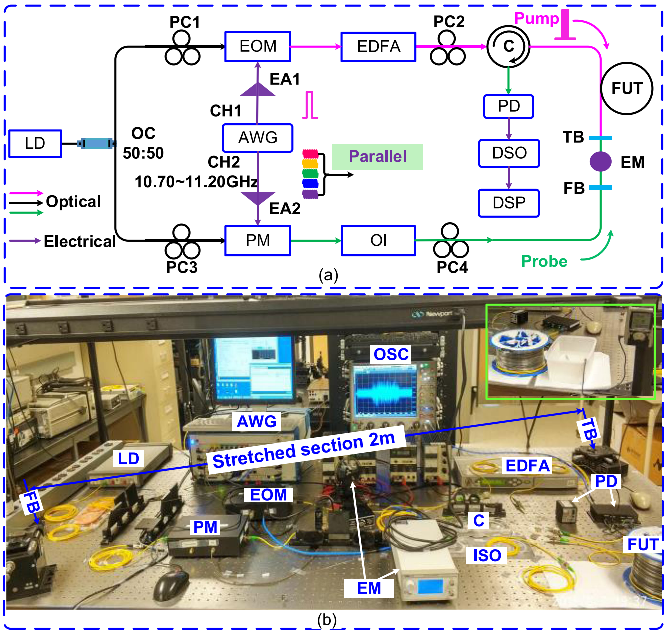

Fig. 2. (a) Schematic diagram of the proposed microwave photonic fiber-optic sensor. (b) A picture showing the experimental setup. Insert in (b) shows temperature measurement setup. LD, laser diode; PC, polarization controller; PM, phase modulator; EOM, electro-optic modulator; AWG, arbitrary waveform generator; EDFA, erbium-doped fiber amplifier; OI, optical isolator; FUT, fiber under test; C, optical circulator; PD, photodetector; DSO, digital storage oscilloscope; DSP, digital signal processing; EA, electrical amplifier; EM, electro-motor; FB, fixed base; TB, tunable base.

in the upper branch being used to generate the optical pump pulse while that in the lower-branch being used to generate the phase-modulated probe wave.

In the upper branch, the CW light wave is converted to an optical pulse by an electro-optic modulator (EOM) driven by a 10-ns electrical pulse generated by an AWG (Keysight M8195A). Then, the optical pulse is amplified up to 34 dBm by an erbium-doped fiber amplifier (EDFA) and used as the pump pulse. The light wave with a power of 1.70 dBm in the lower branch is modulated by an MMT signal, also generated by the AWG at a PM. Both the pump pulse and the phase-modulated probe wave are counter-propagating in a ∼49.5-m PMF. The polarization of the light waves is all aligned along the x-polarization axis of the optical devices. Note that both the electrical pump pulse and the MMT signal output from the AWG are synchronized by a synchronization module (Keysight, M8197A).

The phase-modulated probe wave is transmitted via an optical circulator to a PD (OEQuest, LR-12-A-M, 0.01-15 GHz). The regenerated MMT signal from the PD is acquired by a digital storage oscilloscope (Keysight DSO-Z 504A) with a bandwidth of 63 GHz and a sampling rate of 160 GSa/s. Then, the MMT signal is offline-processed by a computer.

Based on (1), a waveform consisting of 51 sinusoidal microwave signals with the frequencies ranging from 10.700 to 11.200 GHz is edited and stored into the memory of the AWG. The output of the AWG is used as the MMT signal, as shown in Fig. 3(a). Then, the MMT signal is used to phase-modulate the

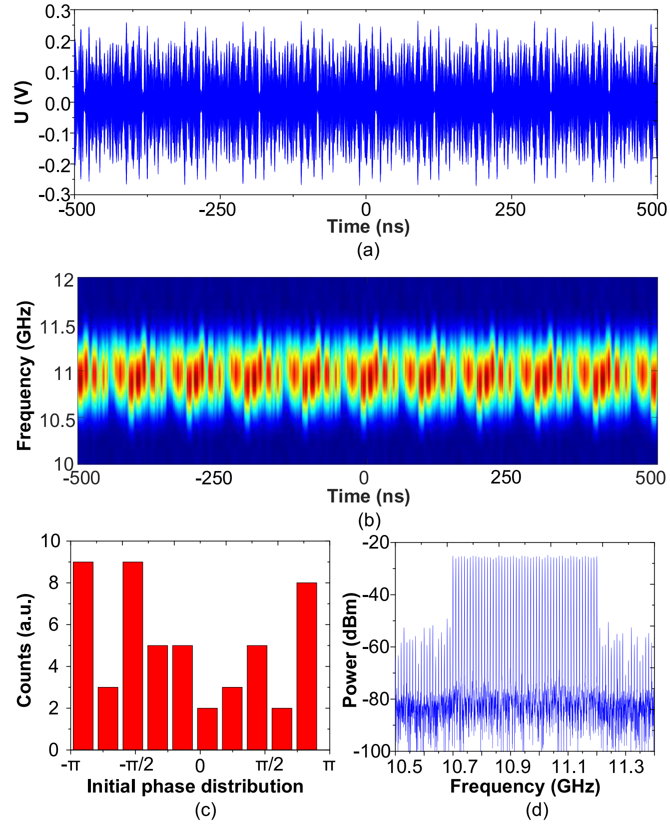

Fig. 3. (a) The waveform and (b) the short-time Fourier transform of the input MMT signal with (c) a randomized initial phase distribution and (d) its electrical power spectrum.

probe wave. As shown in Fig. 3(b), the power spectral density distribution of the short-time Fourier transform is random and uneven because the initial phase of each tone of the MMT signal is randomized, see the distribution in Fig. 3(c). A relatively low PAPR of 9.46 dB is obtained, and, ideally, it will be lower as the tone number increases. As can be seen from the electrical power spectrum in Fig. 3(d), the frequency span of the MMT signal is from 10.700 to 11.200 GHz with a frequency interval of 10 MHz.

The optical power spectrum of the phase-modulated probe wave is measured by an optical spectrum analyzer (OSA, Ando AQ6317B) as shown in Fig. 4. Compared to the optical carrier (blue line) without phase modulation, optical sidebands are generated. The 2nd-order sidebands are 8.8 dB lower than the 1st order sidebands and the higher-order sidebands are much lower than the 1st order sidebands. To eliminate the RF noise generated by the 2nd-order and higher-order sidebands, the regenerated MMT signal is processed by a digital passband filter in the demodulation process for BGS acquisition.

IV. Experimental Results

A. Static Measurement of the Proposed Fiber-Optic Sensor

We evaluate the operation of the proposed fiber-optic sensor for static strain measurement. To measure the strain, a section of 2 m of the PMF is stretched by applying different levels of strain.

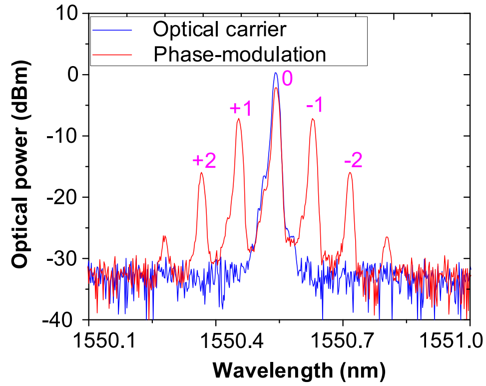

Fig. 4. The power spectrum of the phase-modulated optical probe wave.

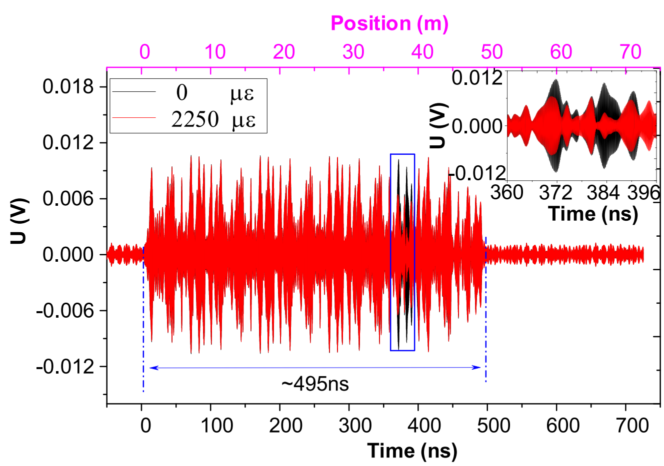

Fig. 5. The regenerated MMT signals corresponding to no strain (black line) and a strain of 2250 $\mu\varepsilon$ (red line). Inset is a zoom-in view of the signals in the blue box.

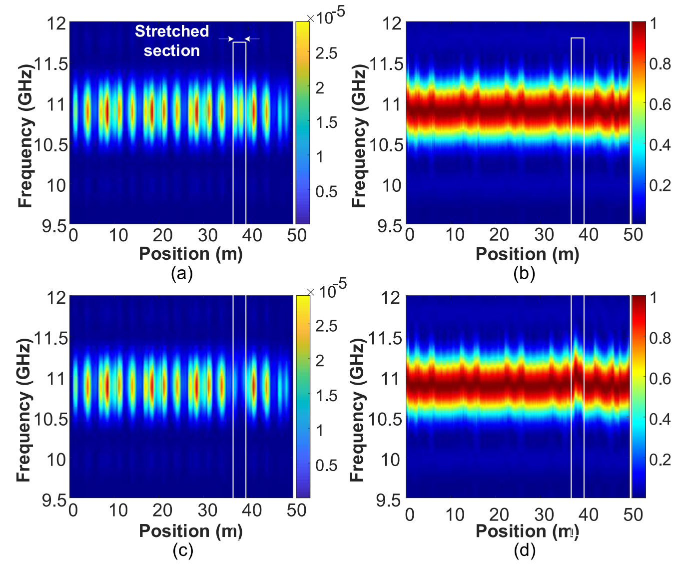

Fig. 6. (a) The BGS distribution and (b) its normalized distribution for the case of no strain; (c) The BGS distribution and (d) its normalized distribution for the case of a strain of 2250 $\mu\varepsilon$. The BGS distribution corresponding to the stretched section is located within the two white lines.

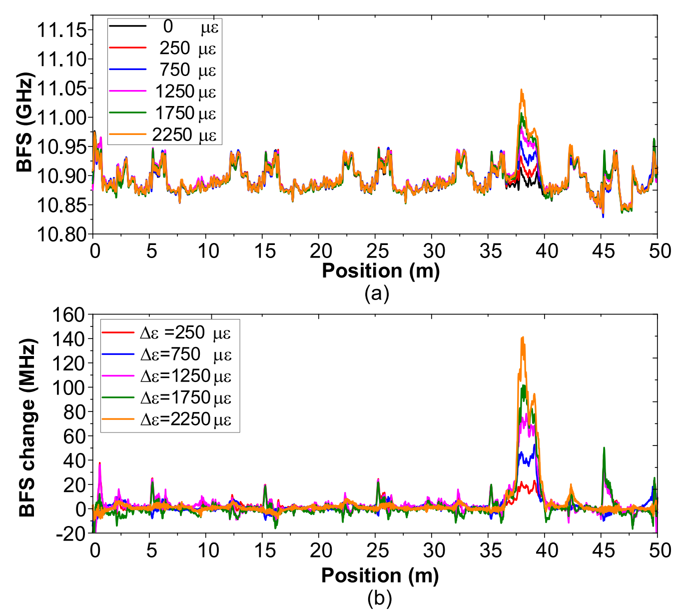

Fig. 7. (a) The BFS distributions versus the position for different strains applied to the PMF. (b) The distributions of the BFS by subtracting the initial BFS distribution.

The width of the pump pulse is set at 10 ns, which is small to ensure a high spatial resolution. The regenerated MMT signals are measured with 512 times averaging, and then it is filtered by a digital filter with a passband from 10.0 to 11.8 GHz, to increase the signal-to-noise ratio (SNR). Two regenerated MMT signals corresponding to no strain and a strain of 2250 $\mu\varepsilon$ are shown in Fig. 5. Since the magnitude and the phase of the regenerated MMT signal are shaped by the complex BGS, the waveform of the regenerated MMT signal with a slightly lower PAPR of 9.24 dB is different from that in Fig. 3(b). It is clearly shown that the MMT signal is amplified from 0 ns to 495 ns corresponding to 49.5 m of the PMF. The two waveforms are overlapped except a portion in a blue box (a zoom-in view in the insert) corresponding to the PMF from 37 to 39 m where the fiber is stretched.

The regenerated MMT signals are demodulated to reconstruct the BGS by STFT with a time window of 10 ns. Based on Eq. (13), the spatial resolution of the proposed sensor is calculated to be 2 m. Two BGS distributions for the two cases of no strain and a strain of 2250 $\mu\varepsilon$ are displayed in Fig. 6(a) and (c), respectively. The power fluctuation of the BGS along the PMF is induced by the non-uniform envelopes of the regenerated MMT signals. Then, the normalized BGS distributions are illustrated in Fig. 6(b) and (d). The stretched section is identified between the two white lines where the BGS is clearly up-shifted as the strain increases. It can be concluded that both the magnitude and the frequency span of the MMT signals are reshaped by the active Brillouin-based MPF when the strain applied to the PMF changes.

Subsequently, the BGSs are fitted based on a Lorentzian-curve function to obtain its center frequencies (i.e., the BFS). The BFS distributions are shown in Fig. 7(a), in which the BFSs at

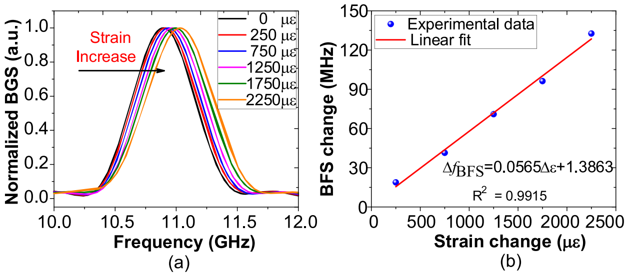

Fig. 8. (a) The BGSs versus the strain change, and (b) the BFS change versus the strain change.

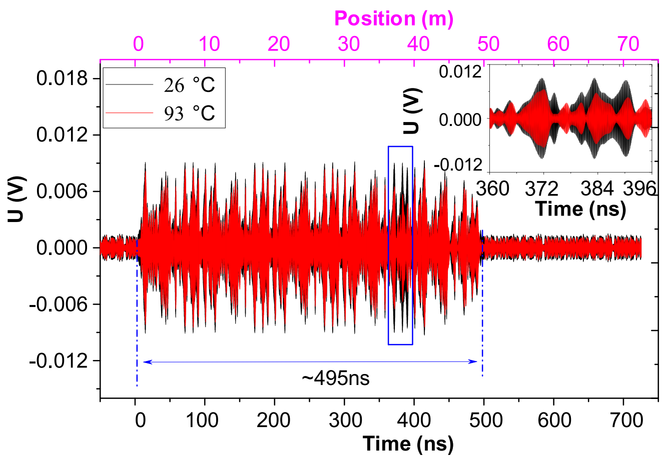

Fig. 9. The regenerated MMT signals for the section of 2 m fiber at a temperature of 26 °C (black line) and 93 °C (red line).

the stretched section are laterally shifted as the strain increases. To eliminate BFS fluctuations, the distributions of the BFSs are computed by subtracting the initial BFS distribution (0 $\mu\varepsilon$) from all the BFS distributions, which are shown in Fig. 7(b).

To observe the dependence of the BGS and the applied strain, the BGS with a 16-points averaging around the position 38.11 m are plotted in Fig. 8(a). It is clearly shown that the BGSs are right-shifted as the strain increase from 0 to 2250 $\mu\varepsilon$. Then, the dependence of the BFS change on the strain change is shown in Fig. 8(b). By linear fitting, a strain coefficient $C_\varepsilon = 0.0565\,\text{MHz}/\mu\varepsilon$ and a high correlation coefficient (R^2) of 0.9915 are obtained.

We also evaluate the static measurement of the proposed fiber-optic sensor for temperature sensing. To do so, the section of 2-m fiber without stretching is embedded in water in a water bath (shown in the inset of Fig. 2). The regenerated MMT signals for a temperature at 26 °C (black line) and 93 °C (red line) are shown in Fig. 9. The waveforms in the inset are apparently shifted as the temperature is increased.

Then, the regenerated MMT signals are demodulated by STFT, and the BGS distributions for the temperatures at 26 °C and 93 °C are shown in Fig. 10(a)) and (c), respectively. Their normalized BGS distributions are illustrated in Fig. 10(b) and (d). The BGS between the two white lines (i.e., the heated section) is up-shifted as the temperature is increased from 26 °C to 93 °C.

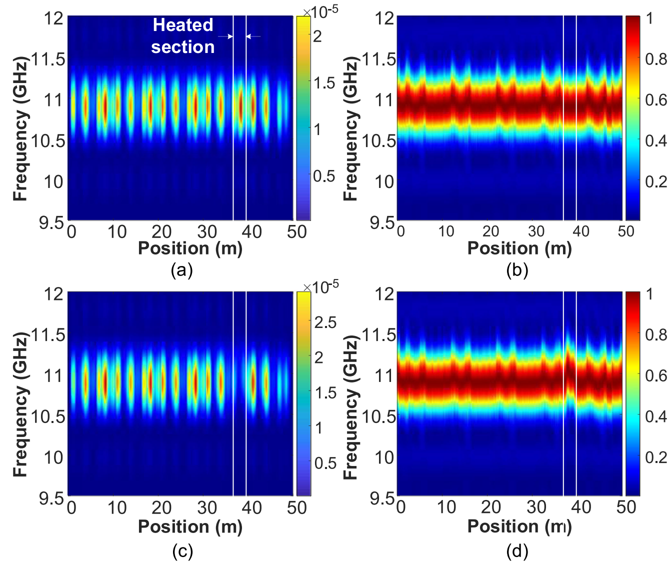

Fig. 10. (a) The BGS distribution and (b) its normalized distribution for the temperature at 26 °C; (c) The BGS distribution and (d) its normalized distribution for the temperature at 93 °C.

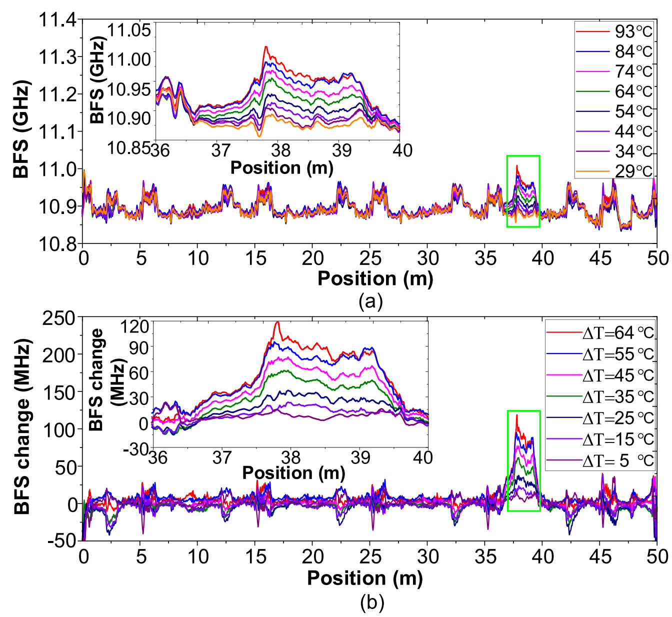

Fig. 11. (a) The BFS distribution and (b) the distribution of the BFS change versus the position for different temperature. Inset is the zoom-in view of the heated section.

Subsequently, the BGSs are fitted based on a Lorentzian-curve function to calculate the BFSs, as shown in Fig. 11(a), in which the BFSs at the heated section are up-shifted. To eliminate the unwanted fluctuation over the BFS distribution, the distributions of the BFS change with a much flat background are calculated by subtracting the initial BFS curve (29 °C) from all the BFS distributions, and they are shown in Fig. 11(b). Then, to further improve the SNR of the BGS, 16 BGS measurements near 38.11 m are averaged, and the averaged BGSs are plotted in Fig. 12(a), which shows a right shift as the temperature increases

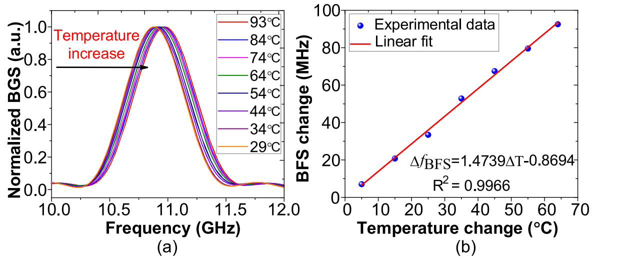

Fig. 12. (a) The BGSs and (b) the BFS changes versus temperature change.

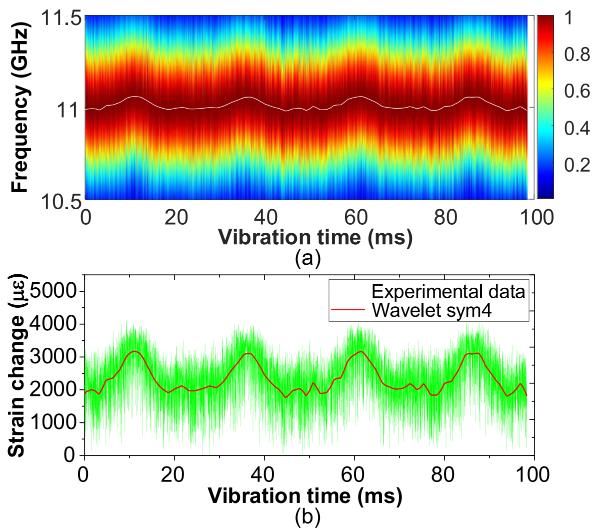

Fig. 13. (a) The time evolution of the BGS (the central white line is the BFS with a denoising method of wavelet sym4). (b) The demodulated vibration waveform.

from 29 °C to 93 °C. The BFS changes over the temperature changes are linearly fitted in Fig. 12(b) resulting in a temperature coefficient $C_T = 1.4739\,\mathrm{MHz}/^{\circ}\mathrm{C}$ and a correlation coefficient (R^2) of 0.9966.

B. Vibration Measurement

To test the ability of the proposed sensor for ultra-fast measurements, an electrical motor (EM) is employed to apply a periodic mechanical vibration to the 2-m section of the PMF. Without averaging, the regenerated MMT signals are measured at a sampling rate of 83.3 kHz. It should be pointed out that the maximum sampling rate of this sensor can reach up to 2 MHz which is inversely proportional to the round-trip time of the PMF in theory, but it is limited by the repetition rate of the pump pulse output from the AWG in the experiment. As shown in Fig. 13(a), the time evolution of the BGS at one point within the vibration position is demodulated. It is clearly seen that the whole BGS is periodically shifted along the vibration time. The mechanical vibration waveform, i.e., the strain curve (green) is illustrated in Fig. 13(b), which has a vibration frequency of 33 Hz. Then, the demodulated BFS of the BGS and the strain curve are post-processed by a denoising method of wavelet sym4 with level 7, achieving an SNR improvement of 27 dB, which corresponds to the white line in Fig. 13(a) and the red line in Fig. 13(b).

V. Conclusion and Discussion

In this work, a microwave photonic fiber-optic sensor has been proposed based on the distributed bandpass MPF to obtain truly distributed and ultra-fast measurement. An MMT signal was modulated on the probe wave and it can be filtered out by a counter-propagating active Brillouin-based MPF with its passband being the convolution between the local BGS of the sensing fiber and the power spectrum of the pump pulse, leading to a regenerated MMT signal. Without averaging, the single measurement can be completed by injecting one single-shot pump pulse so that the sampling rate is only limited by the sensing fiber length. The Brillouin information containing the local temperature or strain is down-converted from the optical domain to the microwave domain, and it can be demodulated by time-frequency analyzing the regenerated MMT signal with STFT. The dynamic range of the proposed sensor can be enlarged by increasing the bandwidth of the input MMT signal. Since the MMT signal consists of multiple single-tone signals with a random initial phase distribution, truly distributed strain and temperature measurements were realized at a high spatial resolution of 2 m which is an order of magnitude higher than that based on the OFDM scheme [17]. Finally, a periodical mechanical vibration with a vibration frequency of 33 Hz is measured at a high sampling rate of 83.3 kHz, with its strain curve being effectively denoised by wavelet sym4. Furthermore, some denoising methods such as image restoration [27] and video-BM3D algorithm [28] can also be used to improve the SNR for ultra-fast vibration measurements.

It should be pointed out that a trade-off between the time (or spatial) resolution and the frequency resolution (measurement errors) exists when using the STFT demodulation process. As shown in Fig. 14, the root mean squared error (RMSE) of the demodulated BFS for static strain measurements can be decreased as the time window of the STFT algorithm is increased. When the time window of the STFT algorithm is 10 ns (corresponding to a high spatial resolution of 2 m), a large RMSE of 22.9 MHz is resulted. When the time window of the STFT algorithm is increased to 200 ns (corresponding to a high spatial resolution of 21 m), a small RMSE of 1.5 MHz is achieved, which is comparable with an ordinary or a coherent BOTDA system and the optical frequency comb schemes such as the OFDM scheme [17] and the DOFC scheme [18], [19]. In the future work, by using a frequency-agile demodulation approach [29] instead of the STFT algorithm, a higher spatial resolution and higher frequency resolution measurements may be obtained. Furthermore, if the MMT signal has a narrower frequency interval and a more uniform initial phase distribution, the non-uniformity of the envelope of the regenerated MMT signal can be effectively mitigated and the unwanted BFS fluctuation could be reduced.

A comparative analysis with existing schemes is shown in Table I. For the regular Brillouin time-domain analysis (BOTDA), coherent BOTDA, and OFA-based BOTDA, multiple pump pulses and the corresponding probe frequency segments are injected into the sensing fiber to complete the frequency sweeping process, which is time-consuming. However, the frequency sweeping process can be realized by launching a

TABLE I
COMPARATIVE ANALYSIS OF THE EXISTING SCHEMES

Schemes	Frequency switch time	Pump pulse number	Dynamic range	Limitation of the spatial resolution	Truly distribution
Ordinary BOTDA [1]	~ms	~50	~100 MHz	Pulse width (1 m)	Yes
Coherent BOTDA [30]	~ms	51	200 MHz	Pulse width (3 m)	Yes
OFA-based BOTDA [13]	~ns	100	200 MHz	Pulse width (1.3 m)	Yes
Single-slope-assisted BOTDA [14]	0	1	~35 MHz	Pulse width (3 m)	Yes
Multi-slope-assisted BOTDA [15]	~ns	~5	330 MHz	Pulse width (1 m)	Yes
OFDM-BOTDA [17]	0	1	1250 MHz	Symbol period (20.48 m)	No
OCC-BOTDA [20]	~ns	1	400 MHz	Chirp duration (2 m)	No
The proposed BOTDA	0	1	500 MHz	Pulse width and time window (2 m)	Yes

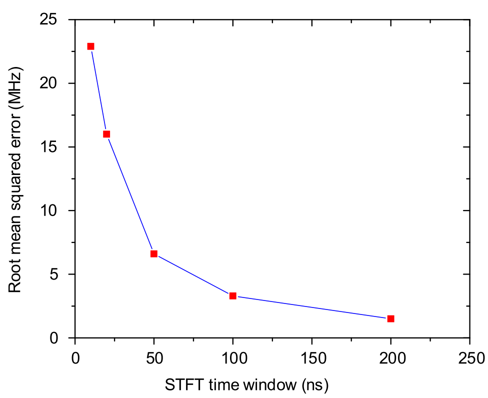

Fig. 14. The RMSE of the demodulated BFS versus the time window of the STFT algorithm.

single-shot pump pulse for the proposed sensor. The slope-assisted BOTDAs have suffered from the tradeoff between sampling rate and wide dynamic range while the single-shot measurement with a wide dynamic range can be obtained by the proposed sensor. Unlike the symbol-by-symbol BGS distribution for the OFDM-BOTDA and the OCC-BOTDA, a truly distributed measurement with a 2-m spatial resolution is obtained for the proposed sensor by moving the time window of the STFT algorithm, and its spatial resolution can be easily tuned by changing the time window of the STFT algorithm.

We believe that the proposed sensor can provide ultra-fast truly distributed measurement with a wide dynamic range and high spatial resolution for practical applications such as health monitoring of large infrastructure, geological hazards prevention, and perimeter security protection.

REFERENCES

[1] X. Bao and L. Chen, "Recent progress in distributed fiber optic sensors," *Sensors*, vol. 12, no. 7, pp. 8601–8639, Jul. 2012.

[2] H. Zhang *et al.*, "Recent progress in fast distributed Brillouin optical fiber sensing," *Appl. Sci.*, vol. 8, no. 10, Feb. 2018, Art. no. 1820.

[3] Z. He, Q. Liu, and T. Tokunaga, "Ultrahigh resolution fiber-optic quasi-static strain sensors for geophysical research," *Photon. Sensors*, vol. 3, no. 4, pp. 295–303, Dec. 2013.

[4] X. Liu, B. Jin, Q. Bai, Y. Wang, D. Wang, and Y. Wang, "Distributed fiber-optic sensors for vibration detection," *Sensors*, vol. 16, no. 8, Jul. 2016, Art. no. 1164.

[5] R. W. Boyd, *Nonlinear Optics*, 3rd ed., Burlington, ON, CA: Academic Press, 2008.

[6] M. Soto, G. Bolognini, and F. Di Pasquale, "Optimization of long-range BOTDA sensors with high resolution using first-order bi-directional Raman amplification," *Opt. Express*, vol. 19, no. 5, pp. 4444–4457, Feb. 2011.

[7] Y. Dong *et al.*, "150 km fast BOTDA based on the optical chirp chain probe wave and Brillouin loss scheme," *Opt. Lett.*, vol. 43, no. 19, pp. 4679–4682, Oct. 2018.

[8] G. P. Agrawal, *Nonlinear Fiber Optics*, 4th ed., Amsterdam, The Netherlands: Elsevier Academic Press, 2007.

[9] K. Hotate and T. Hasegawa, "Measurement of Brillouin gain spectrum distribution along an optical fiber using a correlation-based technique–proposal, experiment and simulation," *IEICE Trans. Electron., C*, vol. 83, no. 3, pp. 405–412, Mar. 2000.

[10] K. Y. Song and K. Hotate, "Distributed fiber strain sensor with 1-kHz sampling rate based on Brillouin optical correlation domain analysis," *IEEE Photonic. Tech. Lett.*, vol. 19, no. 23, pp. 1928–1930, Nov. 2007.

[11] Z. Chunyu, K. Masato, and H. Kazuo, "5,000 points/s high-speed random accessibility for dynamic strain measurement at arbitrary multiple points along a fiber by Brillouin optical correlation domain analysis," *Appl. Phys. Express*, vol. 8, no. 4, Mar. 2015, Art. no. 042501.

[12] K. Y. Song, M. Kishi, Z. He, and K. Hotate, "High-repetition-rate distributed Brillouin sensor based on optical correlation-domain analysis with differential frequency modulation," *Opt. Lett.*, vol. 36, no. 11, pp. 2062–2064, Jun. 2011.

[13] Y. Peled, A. Motil, and M. Tur, "Fast Brillouin optical time domain analysis for dynamic sensing," *Opt. Express*, vol. 20, no. 8, pp. 8584–8591, Apr. 2012.

[14] R. Bernini, A. Minardo, and L. Zeni, "Dynamic strain measurement in optical fibers by stimulated Brillouin scattering," *Opt. Lett.*, vol. 34, no. 17, pp. 2613–2615, Sep. 2009.

[15] D. Ba *et al.*, "Distributed measurement of dynamic strain based on multi-slope assisted fast BOTDA," *Opt. Express*, vol. 24, no. 9, pp. 9781–9793, May 2016.

[16] C. Zhao *et al.*, "BOTDA using channel estimation with direct-detection optical OFDM technique," *Opt. Express*, vol. 25, no. 11, pp. 12698–12709, May 2017.

[17] J. Fang, P. Xu, Y. Dong, and W. Shieh, "Single-shot distributed Brillouin optical time domain analyzer," *Opt. Express*, vol. 25, no. 13, pp. 15188–15198, Jun. 2017.

[18] C. Jin *et al.*, "Scanning-free BOTDA based on ultra-fine digital optical frequency comb," *Opt. Express*, vol. 23, no. 4, pp. 5277–5284, Feb. 2015.

[19] C. Jin *et al.*, "Single-measurement digital optical frequency comb based phase-detection Brillouin optical time domain analyzer," *Opt. Express*, vol. 25, no. 8, pp. 9213–9224, Apr. 2017.

[20] D. Zhou *et al.*, "Single-shot BOTDA based on an optical chirp chain probe wave for distributed ultrafast measurement," *Light: Sci. Appl.*, vol. 7, no. 1, pp. 1–11, Jul. 2018.

[21] Q. Yang, A. A. Amin, and W. Shieh, "Optical OFDM basics," in *Impact of Nonlinearities on Fiber Optic Communications*, S. Kumar, ed., New York, NY, USA: Springer, 2011, pp. 43–85.

[22] R. Tao, X. Feng, Y. Cao, Z. Li, and B. O. Guan, "Widely tunable single bandpass microwave photonic filter based on phase modulation and stimulated Brillouin scattering," *IEEE Photon. Tech. Lett.*, vol. 24, no. 13, pp. 1097–1099, Apr. 2012.

[23] H. Jiang *et al.*, "Wide-range, high-precision multiple microwave frequency measurement using a chip-based photonic Brillouin filter," *Optica*, vol. 3, no. 1, pp. 30–34, Jan. 2016.
[24] D. Marpaung *et al.*, "Low-power, chip-based stimulated Brillouin scattering microwave photonic filter with ultrahigh selectivity," *Optica*, vol. 2, no. 2, pp. 76–83, Feb. 2015.
[25] X. S. Yao, "Phase-to-amplitude modulation conversion using Brillouin selective sideband amplification," *IEEE Photon. Tech. Lett.*, vol. 10, no. 2, pp. 264–266, Feb. 1998.
[26] J. Urricelqui, A. Zornoza, M. Sagues, and A. Loayssa, "Dynamic BOTDA measurements based on Brillouin phase-shift and RF demodulation," *Opt. Express*, vol. 20, no. 24, pp. 26942–26949, Nov. 2012.
[27] M. A. Soto, J. A. Ramírez, and L. Thévenaz, "Intensifying the response of distributed optical fibre sensors using 2D and 3D image restoration," *Nature Commun.*, vol. 7, no. 1, Mar. 2016, Art. no. 10870.
[28] B. Wang, L. Wang, C. Yu, and C. Lu, "Long-distance BOTDA sensing systems using video-BM3D denoising for both static and slowly varying environment," *Opt. Express*, vol. 27, no. 25, pp. 36100–36113, Dec. 2019.
[29] B. Wang *et al.*, "Fast brillouin optical time-domain reflectometry based on the frequency-agile technique," *J. Lightw. Technol.*, vol. 38, no. 4, pp. 946–952, Oct. 2019.
[30] Z. Li, L. Yan, L. Shao, W. Pan, and B. Luo, "Coherent BOTDA sensor with intensity modulated local light and IQ demodulation," *Opt. Express*, vol. 23, no. 12, pp. 16407–16415, Jun. 2015.

Dengwang Zhou was born in Shandong, China, in April 1989. He received the B.S. degree in electronic information science and technology from the Inner Mongolia University of Technology, Hohhot, Mongolia, in 2012 and the M.S. degree in physical electronics from the Harbin Institute of Technology (HIT), Harbin, China, in 2014. He is currently working toward the Ph.D. degree in physical electronics with HIT. Since 2012, he has been researching on fiber-optic sensing group with the School of Aeronautics of HIT. From 2018 to 2019, he has been a Visiting Ph. D. Student with the University of Ottawa, Ottawa, ON, Canada in the Microwave Photonics Research Laboratory. His research interests are in fiber-optic sensors and microwave photonics. He is a Student Member of the Optical Society of America.

Yongkang Dong (Member, IEEE) was admitted into the Harbin Institute of Technology (HIT), Harbin, China, in 1999 majored in physical electronics and received the bachelor's degree and the Ph.D. degrees in 2003 and 2008, respectively. From 2008 to 2011, he was working as a Postdoctoral Fellow with the Physics Department, University of Ottawa, Canada. In 2012, he re-joined HIT as a Full Professor. He has authored and co-authored more than 80 international journal papers. His current research interests involve nonlinear fiber optics and Brillouin scattering based optical fiber sensors and their applications in structural health monitoring. He is the recipient of the First Prize in Provincial Natural Science Award (2013), the Innovation Award of Chinese Society for Optical Engineering (2015), and the First Prize in Provincial Science and Technology Progress Award (2017). He is currently the Chief Scientist of the National Key Scientific Instrument and Equipment Development Project of China.

Jianping Yao (Fellow, IEEE) received the Ph.D. degree in electrical engineering from the Université de Toulon et du Var, Toulon, France, in December 1997. He is a Distinguished University Professor and the University Research Chair with the School of Electrical Engineering and Computer Science, University of Ottawa, Ottawa, ON, Canada. From 1998 to 2001, he was with the School of Electrical and Electronic Engineering, Nanyang Technological University, Singapore, as an Assistant Professor. In December 2001, he joined the School of Electrical Engineering and Computer Science, University of Ottawa, as an Assistant Professor, where he was promoted to an Associate Professor in May 2003, and a Full Professor in May 2006. He was appointed the University Research Chair in Microwave Photonics in 2007. In June 2016, he was conferred the title of Distinguished University Professor of the University of Ottawa. From July 2007 to June 2010 and July 2013 to June 2016, he was the Director of the Ottawa-Carleton Institute for Electrical and Computer Engineering. He has authored or co-authored more than 620 papers including more than 360 papers in peer-reviewed journals and more than 260 papers in conference proceedings. He is an Editor-in-Chief for the *IEEE Photonics Technology Letters*, a former Topical Editor of *Optics Letters*, an Associate Editor for *Science Bulletin*, a Steering Committee Member of IEEE/OSA JOURNAL OF LIGHTWAVE TECHNOLOGY, and an Advisory Editorial Board member of *Optics Communications*. He was a Guest Editor of a Focus Issue on Microwave Photonics in *Optics Express* in 2013, a Lead-Editor of a Feature Issue on Microwave Photonics in *Photonics Research* in 2014, and a Guest Editor of a Special Issue on Microwave Photonics in IEEE/OSA JOURNAL OF LIGHTWAVE TECHNOLOGY in 2018. He is currently the Technical Committee Chair of IEEE MTT-3 Microwave Photonics and an elected member of the Board of Governors of the IEEE Photonics Society (2019–2021). He was a member of the European Research Council Consolidator Grant Panel in 2016 and 2018, the Qualitative Evaluation Panel in 2017, and a panelist of the National Science Foundation Career Awards Panel in 2016.. He is a Fellow of the Optical Society of America (OSA), the Canadian Academy of Engineering (CAE), and the Royal Society of Canada (RSC). He was the Chair of a number of international conferences, symposia, and workshops, including the Vice Technical Program Committee (TPC) Chair of the 2007 IEEE Topical Meeting on Microwave Photonics, TPC Co-Chair of the 2009 and 2010 Asia-Pacific Microwave Photonics Conference, TPC Chair of the high-speed and broadband wireless technologies subcommittee of the IEEE Radio Wireless Symposium 2009-2012, TPC Chair of the microwave photonics subcommittee of the IEEE Photonics Society Annual Meeting 2009, TPC Chair of the 2010 IEEE Topical Meeting on Microwave Photonics, the General Co-Chair of the 2011 IEEE Topical Meeting on Microwave Photonics, TPC Co-Chair of the 2014 IEEE Topical Meetings on Microwave Photonics, the General Co-Chair of the 2015 and 2017 IEEE Topical Meeting on Microwave Photonics, and the General Chair of the 2019 IEEE Topical Meeting on Microwave Photonics. He was a committee member for a number of international conferences, such as IPC, OFC, CLEO, BGPP, and MWP. He was the recipient of the 2005 International Creative Research Award of the University of Ottawa. He was the recipient of the 2007 George S. Glinski Award for Excellence in Research. In 2008, he was awarded a Natural Sciences and Engineering Research Council of Canada Discovery Accelerator Supplements Award. He was selected to receive an inaugural OSA Outstanding Reviewer Award in 2012 and was one of the top ten reviewers of IEEE/OSA JOURNAL OF LIGHTWAVE TECHNOLOGY 2015–2016. He was the IEEE MTT-S Distinguished Microwave Lecturer for 2013–2015. He received the 2017-2018 Award for Excellence in Research of the University of Ottawa, and was the recipient of the 2018 R.A. Fessenden Silver Medal from IEEE Canada. He is a registered Professional Engineer of Ontario